Supporting Information

Simultaneous Formation of Sulfate and Nitrate via Co-uptake of SO_2 and NO_2 by Aqueous NaCl Droplets: Combined Effect of Nitrate Photolysis and Chlorine Chemistry

Ruifeng Zhang[1,2], Chak K. Chan[1,2,3]*

[1]School of Energy and Environment, City University of Hong Kong, Tat Chee Avenue, Kowloon 999077, Hong Kong, China
[2]Shenzhen Research Institute, City University of Hong Kong, Shenzhen 518057, China
[3]Low-Carbon and Climate Impact Research Centre, City University of Hong Kong, Tat Chee Avenue, Kowloon 999077, Hong Kong, China

Correspondence to: Chak K. Chan (chak.k.chan@cityu.edu.hk)

Text S1. Calculation of Henry's law constant

The effective Henry's law constants of NO_2 and SO_2, denoted by H^*_{NO2} and H^*_{SO2}, respectively, as a function of time, were estimated based on the experimental data points, and the expressions were input into the kinetic model for further simulations.

(1) Calculation of H^*_{NO2}.

Gaseous NO_2 is first absorbed onto the surface of the droplets, followed by diffusion to the bulk of particles, and then participates in a series of reactions afterward. The NO_2 (aq) hydrolysis ($NO_2(aq) + NO_2(aq) + H_2O \rightarrow NO_3^- + NO_2^- + 2\ H^+$, $k_1 = 1.0 \times 10^8\ M^{-1}\ s^{-1}$) would be the sole reaction in forming nitrate during unary uptake of NO_2 under dark. Therefore, the nitrate production rate can be estimated as below:

$$\frac{d[NO_3^-]}{dt} = k_1(H^*_{NO2}P_{NO2})^2 \qquad \text{(Equation 1)}$$

Therefore, H^*_{NO2} can be calculated as below:

$$H^*_{NO2} = \sqrt{\frac{d[NO_3^-]}{dt}/k_1P^2_{NO2}} \qquad \text{(Equation 2)}$$

In the present study, $\frac{d[NO_3^-]}{dt}$ was obtained via solving the differentiation of the $[NO_3^-]$ equation as a function of time. Consequently, H^*_{NO2} can be expressed as a function of time, which was input into the kinetic model for further simulations. For unary/co-uptake experiments under irradiation, the equation derived from unary uptake under dark was adjusted to fit experimentally measured nitrate and sulfate.

(2) Calculation of H^*_{SO2}(Griffiths et al., 2009; Gutzwiller et al., 2002; Kolb et al., 2002; Stewart et al., 2004)

There are a few pathways that could yield sulfate production. Thus, it is difficult to derive the expression of H^*_{SO2} directly with the same method for H^*_{NO2} described above. In this case, we calculated the reactive uptake coefficient of SO_2, γ_{SO2}, from experimentally measured sulfate concentration as follows:

$$\gamma_{SO2} = \frac{d[SO_4^{2-}]}{dt}/Z \qquad \text{(Equation 3)}$$

$$Z = \frac{1}{4}v_{SO2}A_s[SO_2] \qquad \text{(Equation 4)}$$

$$v_{SO2} = \sqrt{8RT/\pi M_{SO2}} \quad \text{(Equation 5)}$$

$$A_s = 4\pi r_p^2 \times (4\pi r_p^3/3)^{-1}\,, \quad \text{(Equation 6)}$$

where $\frac{d[SO_4^{2-}]}{dt}$ was obtained via solving the differentiation of [SO_4^{2-}] equation as a function of time. Finally, we can obtain the expression of γ_{SO2} as a function of time.

Besides, the γ_{SO2} can also be described via the resistor model. According to the theory of gas uptake into liquid aerosol droplets, the measured uptake coefficients are given by Equation 3. Specifically, the canonical kinetic model assumes that gas molecules are accommodated at the surface first, followed by the diffusion from the surface to the bulk where the reaction takes place (Galib and Limmer 2021). The bulk reaction with rate k_h should be slow enough that an equilibrium can be established between the gas and the liquid phase, with concentrations determined by H^*_{SO2}. Under these assumptions for the mass transfer kinetics, the reactive uptake coefficient can be estimated as below:(Galib and Limmer 2021)

$$\frac{1}{\gamma_{SO2}} = \frac{1}{\alpha_{SO2}} + \frac{v_{SO2}}{4H^*_{SO2}RT\sqrt{D_{SO2}k_h}}\left(\coth q - \frac{1}{q}\right)^{-1} \quad \text{(Equation 7)}$$

Where α_{SO2} is the accommodation coefficient of SO_2 (~0.11), v_{SO2} is the thermal velocity in the gas phase, T and R are the absolute temperature and gas constant, respectively, D_{SO2} is the liquid diffusion coefficient (~1.32×10^{-9} m^2 s^{-1}). k_h is a the pseudo-first-order rate constant for the reaction between S(IV) and oxidants (k_h = k_{2nd}[oxidants]). It should be noted that uptake coefficients are measured on a relatively thick liquid film compared to liquid films occurring on aerosol particles (Li et al., 2022), The diffusoreactive length is defined as the distance from the surface where the reaction occurs (Li et al., 2022; Mekic et al., 2018). The (*coth*q-1/q) is the correction factor that should be used to extrapolate the measured uptake coefficients under laboratory conditions to small particles (Li et al., 2022). The parameter q is the ratio of particle radius, r_p, to the reacto-diffusive length, *l*. The reacto-diffusive length, $l=\sqrt{D_{SO2}k_h}$, is a measure of the mean distance from the gas/liquid interface that a molecule diffuses in the droplets before the reaction occurs (Stewart et al., 2004). Therefore, the H^*_{SO2} can be estimated by the equation as follows:

$$H^*_{SO2} = \frac{v_{SO2}(\coth q - \frac{1}{q})^{-1}}{4(\frac{1}{\gamma_{SO2}} - \frac{1}{\alpha_{SO2}})RT\sqrt{D_{SO2}k_h}}$$

As a result, the calculated time profiles of H^*_{SO2} was input into the kinetic model.

Table S1. The mechanisms used in the kinetic model.

Reactions		Rate constant	Note
SR1	$NO_3^- + h\nu + H^+ \rightarrow NO_2 + OH$ $NO_3^- + hv \rightarrow NO_2^- + O(^3P)$	j_{NO3-}	This study
SR2	$N(III) + h\nu + H^+ \rightarrow NO + OH$ $N(III): NO_2^-/HNO_2$	$j_{NO2-} = 2\ j_{NO3-}$ $j_{HNO2} = 10\ j_{NO3-}$	(Gen et al., 2019)
SR3	$NO_2 + NO_2 + H_2O \rightarrow NO_2^- + NO_3^- + 2\ H^+$	1.0×10^8	(Seinfeld and Pandis 2006)
SR4	$NO_2 + OH \rightarrow NO_3^- + H^+$	4.5×10^9	(Benner et al., 1988)
SR5	$NO_2^- + OH \rightarrow NO_2 + OH^-$	1.0×10^{10}	(Scharko et al., 2014)
SR6	$HNO_2 + OH \rightarrow NO_2 + H_2O$	3.0×10^9	(Scharko et al., 2014)
SR7	$NO_2 + NO + H_2O \rightarrow 2\ NO_2^- + 2\ H^+$	2.0×10^8	(Seinfeld and Pandis 2006)
SR8	$NO + OH \rightarrow NO_2^- + H^+$	2.0×10^{10}	(Seinfeld and Pandis 2006)
SR9	$NO_3 + NO_2 \rightarrow N_2O_5$	1.7×10^9	(Katsumura et al., 1991)
SR10	$N_2O_5 \rightarrow NO_2^+ + NO_3^-$	$>1.0 \times 10^4$	(Behnke et al., 1997)
SR11	$NO_2^+ + H_2O \rightarrow NO_3^- + 2\ H^+$	8.9×10^7	(Behnke et al., 1997)
SR12	$NO_2^+ + Cl^- \rightarrow ClNO_2$	3.9×10^{10}	(Behnke et al., 1997)
SR13	$NO_3 + H_2O_2 \rightarrow NO_3^- + H^+ + HO_2$	1.0×10^6	(Seinfeld and Pandis 2006)
SR14	$NO_3 + HO_2 \rightarrow NO_3^- + O_2 + H^+$	4.5×10^9	(Seinfeld and Pandis 2006)
SR15	$OH + OH \rightarrow H_2O_2$	5.5×10^9	(Zhang et al., 2021)
SR16	$O(^3P) + O_2 \rightarrow O_3$	4.0×10^9	(Kläning et al., 1984)
SR17	$OH + O_3 \rightarrow HO_2 + O_2$	1.0×10^8	(Sehested et al., 1984)
SR18	$OH + H_2O_2 \rightarrow HO_2 + H_2O$	2.7×10^7	(Buxton et al., 1988)
SR19	$HSO_3^- + OH \rightarrow SO_3^- + H_2O$	4.5×10^9	(Seinfeld and

			Pandis 2006)
SR20	$SO_3^- + O_2 \rightarrow SO_5^-$	1.5×10^9	(Seinfeld and Pandis 2006)
SR21	$SO_5^- + HSO_3^- \rightarrow HSO_5^- + SO_3^-$	2.5×10^4	(Seinfeld and Pandis 2006)
SR22	$SO_5^- + HSO_3^- \rightarrow SO_4^- + SO_4^{2-} + H^+$	7.5×10^4	(Seinfeld and Pandis 2006)
SR23	$SO_4^- + HSO_3^- \rightarrow SO_4^{2-} + SO_3^- + H^+$	7.5×10^8	(Seinfeld and Pandis 2006)
SR24	$SO_4^- + SO_4^- \rightarrow S_2O_8^{2-}$	4.5×10^8	(Seinfeld and Pandis 2006)
SR25	$SO_4^- + NO_3^- \rightarrow SO_4^{2-} + NO_3$	5.0×10^4	(Løgager et al., 1993)
SR26	$SO_4^- + HO_2 \rightarrow SO_4^{2-} + H^+ + O_2$	5.0×10^9	(Seinfeld and Pandis 2006)
SR27	$SO_4^- + H_2O_2 \rightarrow SO_4^{2-} + H^+ + HO_2$	1.2×10^7	(Seinfeld and Pandis 2006)
SR28	$SO_4^- + OH^- \rightarrow OH + SO_4^{2-}$	8.0×10^7	(Seinfeld and Pandis 2006)
SR29	$SO_4^- + OH \rightarrow HSO_5^-$	9.5×10^9	(Klaning et al., 1991)
SR30	$SO_3^- + SO_3^- \rightarrow S_2O_6^{2-}$	7.0×10^8	(Seinfeld and Pandis 2006)
SR31	$SO_5^- + SO_5^- \rightarrow S_2O_8^{2-} + O_2$	1.4×10^8	(Seinfeld and Pandis 2006)
SR32	$SO_5^- + SO_5^- \rightarrow 2\ SO_4^{2-} + O_2$	6.0×10^8	(Seinfeld and Pandis 2006)
SR33	$HSO_5^- + HSO_3^- + H^+ \rightarrow 2\ SO_4^{2-} + 3\ H^+$	7.1×10^6	(Seinfeld and Pandis 2006)
SR34	$HSO_5^- + SO_4^- \rightarrow SO_5^- + SO_4^{2-} + H^+$	$<1.0 \times 10^5$	(Seinfeld and Pandis 2006)
SR35	$HSO_5^- + OH \rightarrow SO_5^- + H_2O$	1.7×10^7	(Seinfeld and Pandis 2006)
SR36	$HSO_3^- + NO_3 \rightarrow NO_3^- + H^+ + 2\ SO_3^-$	1.4×10^8	(Seinfeld and Pandis 2006)
SR37	$HSO_3^- + H_2O_2 \rightarrow SO_4^{2-} + H_2O$	7.45×10^7	(Seinfeld and Pandis 2006)
SR38	$2\ NO_2 + HSO_3^- + H_2O \rightarrow SO_4^{2-} + 2\ NO_2^- + 3\ H^+$	2.0×10^6	(Seinfeld and Pandis 2006)
SR39	$NO_2^- + HSO_3^- + H^+ \rightarrow NOH + SO_4^{2-} + 2\ H^+$	3.8×10^3	(Gen et al., 2019)
SR40	$Cl^- + h\nu \rightarrow Cl$	j_{Cl^-}	This study
SR41	$Cl^- + OH \leftrightarrow ClOH^-$	$k_f = 4.3 \times 10^9$ $k_r = 6.1 \times 10^9$	(Seinfeld and Pandis 2006)
SR42	$Cl^- + Cl \leftrightarrow Cl_2^-$	$k_f = 6.5 \times 10^9$ $k_r = 6.0 \times 10^4$	(Zhang et al., 2020)
SR43	$Cl + H_2O \leftrightarrow ClOH^- + H^+$	$k_f = 1.3 \times 10^3\ s^{-1}$ $k_r = 2.1 \times 10^{10}$	(Seinfeld and Pandis 2006;

			Zhang et al., 2020)
SR44	$Cl + Cl \rightarrow Cl_2$	8.8×10^7	(Bulman et al., 2019)
SR45	$Cl + Cl_2^- \rightarrow Cl_2 + Cl^-$	2.1×10^9	(Yu and Barker 2003)
SR46	$Cl + NO_3^- \leftrightarrow NO_3 + Cl^-$	$k_f = 1.0 \times 10^8$ $kr = 3.5 \times 10^8$	(Poskrebyshev et al., 2003)
SR47	$Cl + HO_2 \rightarrow Cl^- + O_2 + H^+$	3.1×10^9	(Seinfeld and Pandis 2006)
SR48	$Cl + H_2O_2 \rightarrow Cl^- + HO_2 + H^+$	4.5×10^7	(Seinfeld and Pandis 2006)
SR49	$Cl_2^- + OH \rightarrow HOCl + Cl^-$	1.0×10^9	(Bulman et al., 2019)
SR50	$Cl_2^- + NO_3 \rightarrow NO_3^- + Cl_2$	1.0×10^9	(Poskrebyshev et al., 2003)
SR51	$Cl_2^- + HO_2 \rightarrow 2\ Cl^- + O_2 + H^+$	4.5×10^9	(Seinfeld and Pandis 2006)
SR52	$Cl_2^- + OH^- \rightarrow 2\ Cl^- + OH$	$7.3 \times 10^6\ s^{-1}$	(Seinfeld and Pandis 2006)
SR53	$Cl_2^- + H_2O_2 \rightarrow 2\ Cl^- + HO_2 + H^+$	1.4×10^5	(Seinfeld and Pandis 2006)
SR54	$HOCl \leftrightarrow H^+ + OCl^-$	$k_f = 1.41 \times 10^3\ s^{-1}$ $k_r = 5.0 \times 10^{10}$	(Bulman et al., 2019)
SR55	$Cl^- + HSO_5^- \rightarrow SO_4^{2-} + product$	1.8×10^{-3}	(Seinfeld and Pandis 2006)
SR56	$Cl^- + SO_4^- \leftrightarrow SO_4^{2-} + Cl$	$k_f = 2.0 \times 10^8$ $kr = 2.5 \times 10^8$	(Machulek et al., 2009)
SR57	$Cl + HSO_3^- \rightarrow Cl^- + H^+ + SO_3^-$	3.4×10^9	(Huie and Neta 1987)
SR58	$HOCl + HSO_3^- \rightarrow SO_4^{2-} + Cl^- + 2\ H^+$	7.6×10^8	(Horváth et al., 2006)
SR59	$Cl_2^- + HSO_3^- \rightarrow 2\ Cl^- + H^+ + SO_3^-$	3.4×10^8	(Seinfeld and Pandis 2006)

Table S2. Initial chloride concentration input in the kinetic model.

Exp. #	Experimental conditions	E-AIM predicted $[Cl^-]$ (M)	Corrected $[Cl^-]$ (M)
1	NaCl droplets equilibrated at 80% RH	4.6	3.9
2	NaCl droplets equilibrated at 70% RH	6.2	5.5
3	NaCl droplets equilibrated at 60% RH	7.7	6.3

Table S3. Summary of nitrate photolysis rate constant, j_{NO3-}, and chloride photolysis rate constant, j_{Cl-}.

Conditions	j_{NO3-} (s^{-1})	j_{Cl-} (s^{-1})
NaCl + SO_2 + light at 80% RH	N/A	1.8×10^{-7}
NaCl + SO_2 + light at 70% RH	N/A	4.7×10^{-7}
NaCl + SO_2 + light at 60% RH	N/A	5.6×10^{-7}
NaCl + NO_2 + light at 80% RH	1.2×10^{-6}	5.3×10^{-7}
NaCl + NO_2 + light at 70% RH	1.2×10^{-6}	5.1×10^{-7}
NaCl + NO_2 + light at 60% RH	1.2×10^{-6}	5.0×10^{-7}
NaCl + SO_2 + NO_2 + light at 80% RH	1.4×10^{-6}	3.8×10^{-7}
NaCl + SO_2 + NO_2 + light at 70% RH	1.4×10^{-6}	4.4×10^{-7}
NaCl + SO_2 + NO_2 + light at 60% RH	1.6×10^{-6}	4.1×10^{-7}

Table S4. Sulfate production rate under various conditions.

Exp. #	Experimental conditions	Averaged Sulfate production rate (first stage) ($M \cdot s^{-1}$)	Averaged Sulfate production rate (second stage) ($M \cdot s^{-1}$)
1	NaCl + NO_2 + SO_2 + light + air + 80% RH	1.6×10^{-6}	2.7×10^{-6}
2	NaCl + SO_2 + light + air + 80% RH	1.3×10^{-6}	
3	NaCl + NO_2 + SO_2 + light + air + 70% RH	2.3×10^{-6}	5.9×10^{-6}
4	NaCl + SO_2 + light + air + 70% RH	2.3×10^{-6}	
5	NaCl + NO_2 + SO_2 + light + air + 60% RH	3.1×10^{-6}	8.6×10^{-6}
6	NaCl + SO_2 + light + air + 60% RH	3.3×10^{-6}	
7	NaCl + SO_2 + light (low intensity) + air + 60% RH	1.7×10^{-6}	

Table S5. Uptake coefficient of SO_2, γ_{SO2}, at different RHs.

Exp. #	Experimental conditions	γ_{SO2}, (first stage)	γ_{SO2}, (second stage)
1	NaCl + NO_2 + SO_2 + light + air + 80% RH	$(0.7 \pm 0.12) \times 10^{-6}$	$(1.2 \pm 0.09) \times 10^{-6}$
2	NaCl + SO_2 + light + air + 80% RH	$(0.7 \pm 0.03) \times 10^{-6}$	

3	NaCl + NO_2 + SO_2 + light + air + 70% RH	$(1.1 \pm 0.06) \times 10^{-6}$	$(2.8 \pm 0.06) \times 10^{-6}$
4	NaCl + SO_2 + light + air + 70% RH	$(1.1 \pm 0.08) \times 10^{-6}$	
5	NaCl + NO_2 + SO_2 + light + air + 60% RH	$(1.4 \pm 0.11) \times 10^{-6}$	$(4.0 \pm 0.10) \times 10^{-6}$
6	NaCl + SO_2 + light + air + 60% RH	$(1.4 \pm 0.10) \times 10^{-6}$	

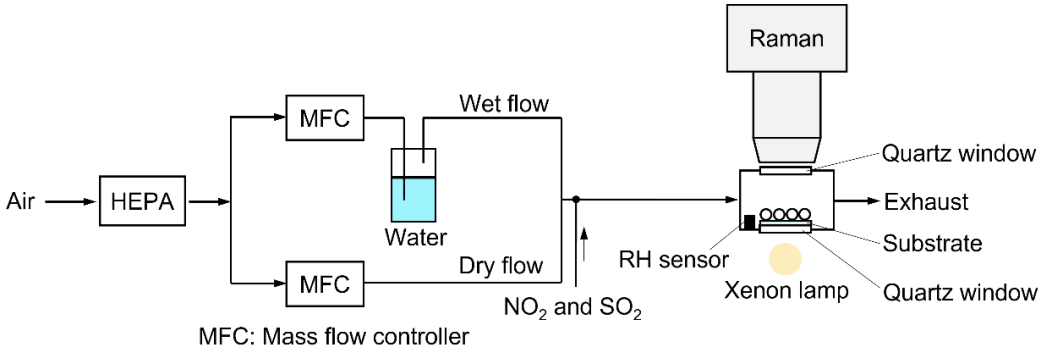

Figure S1. The Raman Spectroscopy/Flow cell setup.

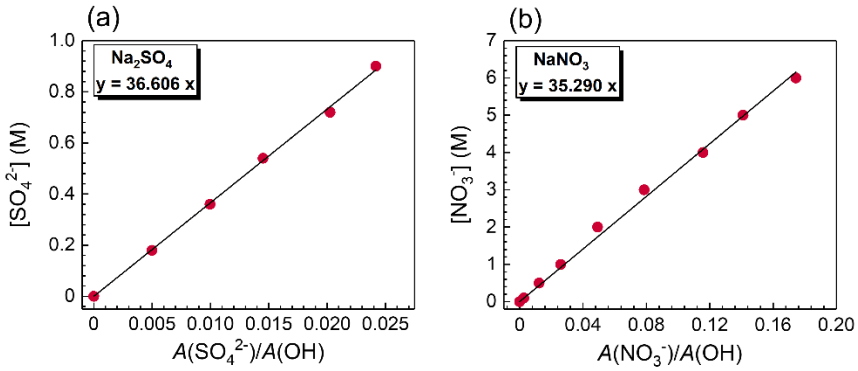

Figure S2. Calibration curve of (a) Na_2SO_4 and (b) $NaNO_3$.

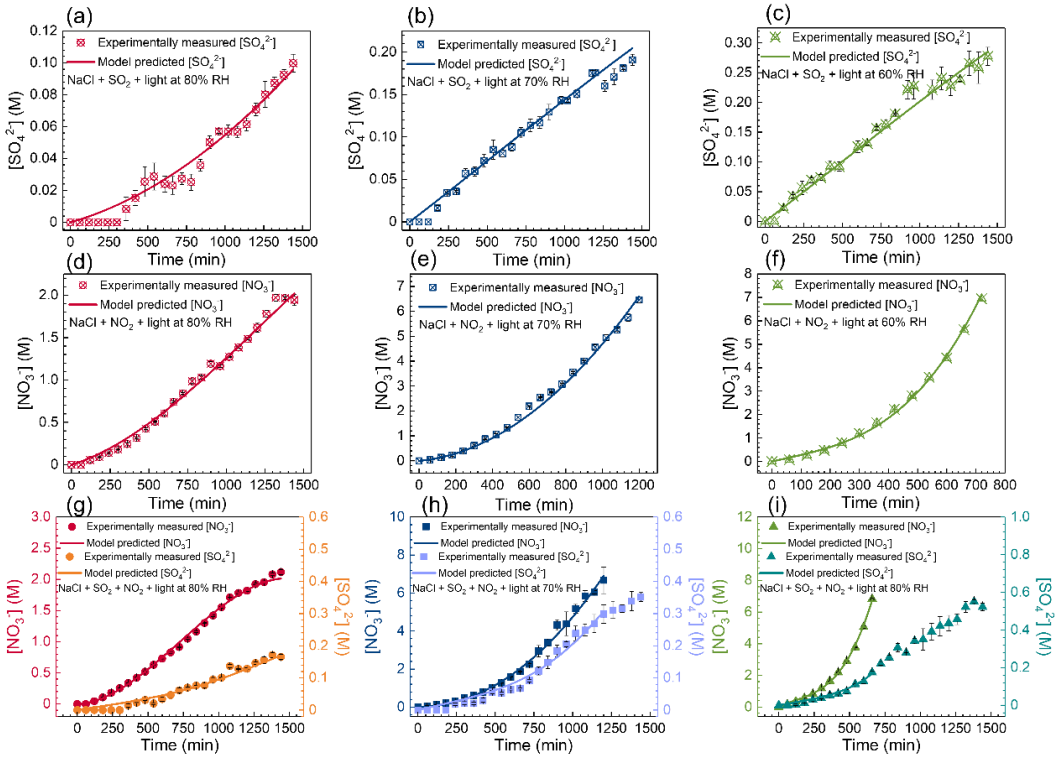

Figure S3. Experimentally measured and model-predicted sulfate and nitrate concentration as a function of time under various conditions.

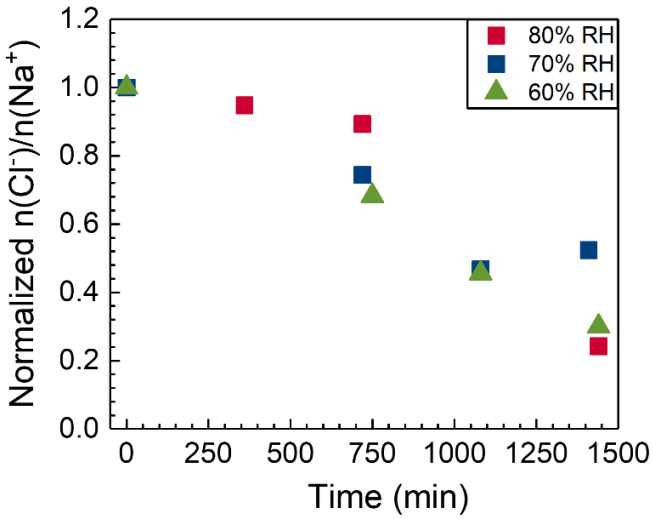

Figure S4. Cl depletion during unary uptake of NO_2 into NaCl droplets under dark. The initial $n(Cl^-)/n(Na^+)$ after equilibrium is 0.84, 0.88, and 0.82 at 60%, 70%, and 80% RH, respectively. The corrected initial Cl^- concentration based on the $n(Cl^-)/n(Na^+)$ was input into the model.

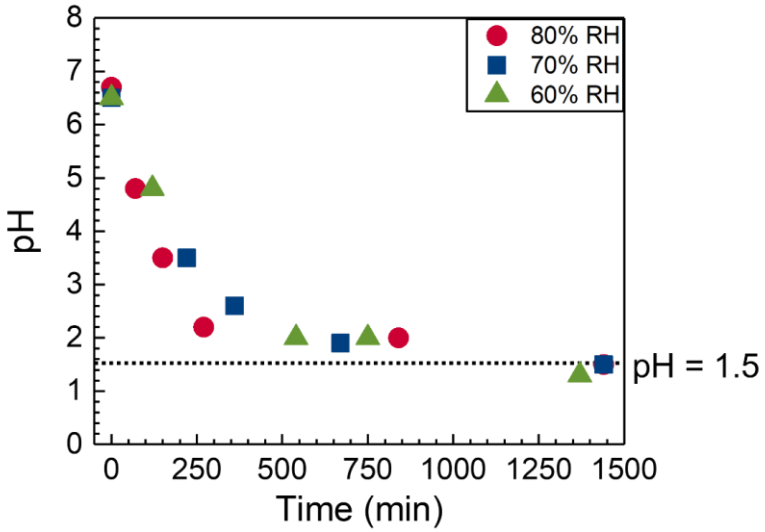

Figure S5. pH as a function of time during the unary uptake of NO_2 into aqueous NaCl droplet under dark at 60%, 70%, and 80% RH. Considering that pH drops quickly at the initial stage and the fast uptake of NO_2, the pH = 1.5 as a fixed value was input into the model under conditions with the involvement of NO_2.

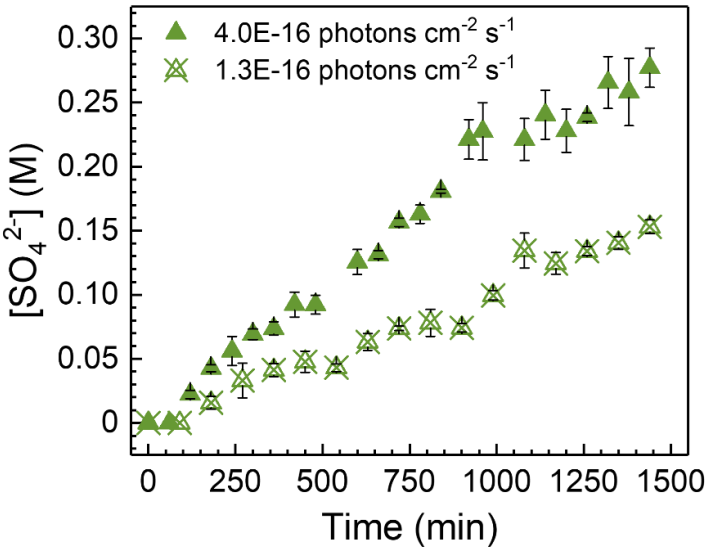

Figure S6. Sulfate concentration as a function of time during the unary uptake of SO_2 into NaCl droplets at 60% RH at different light intensities.

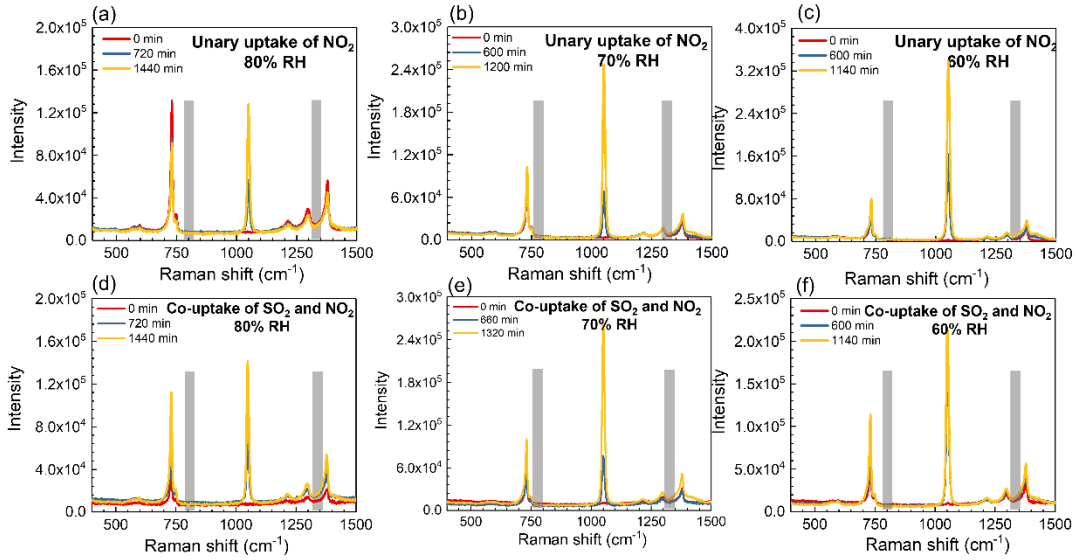

Figure S7. The time profiles of Raman spectra under dark. The shaded area represents the Ramana feature of nitrite.

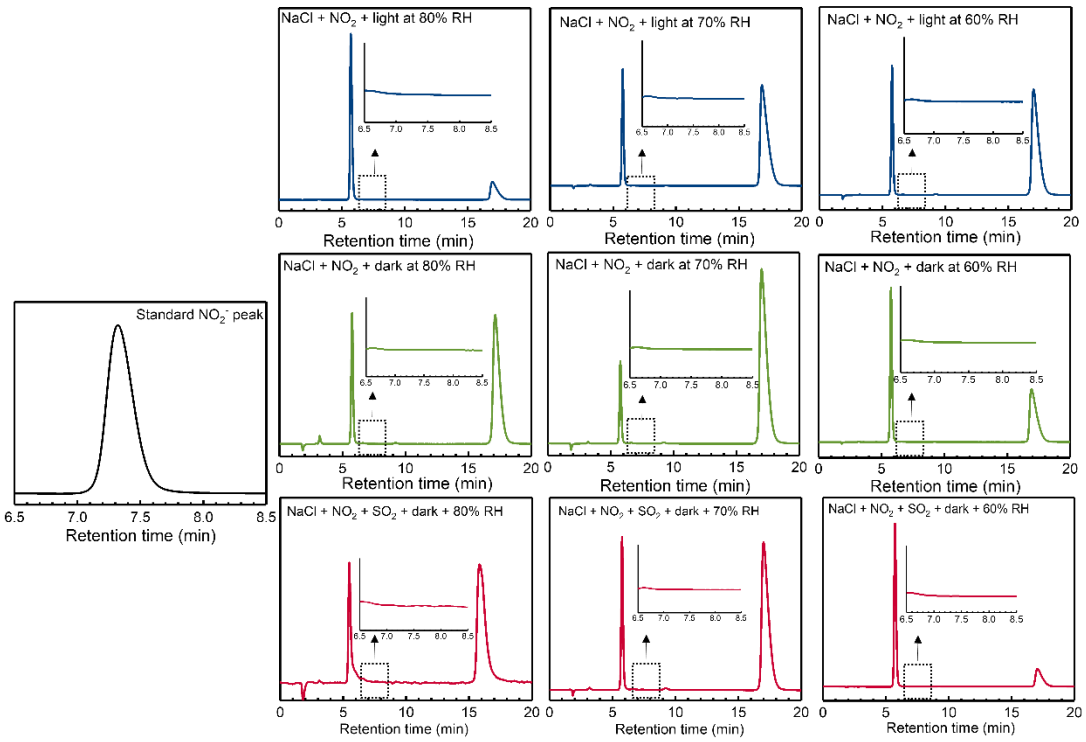

Figure S8. IC measurements.

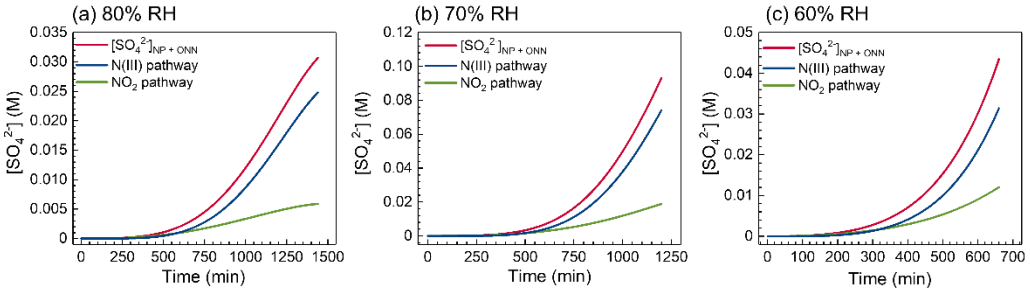

Figure S9. The contribution of N(III) pathway and NO_2 pathway to sulfate production.

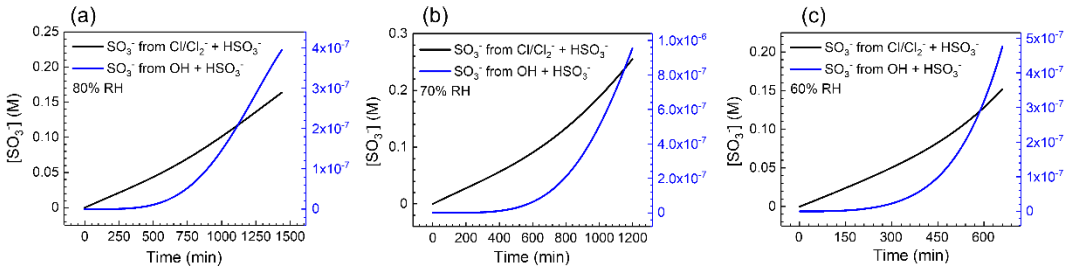

Figure S10. Model predicted SO_3^- concentration from the reaction of $Cl^{\bullet}/Cl_2^{\bullet-}$ + HSO_3^- and $OH + HSO_3^-$.

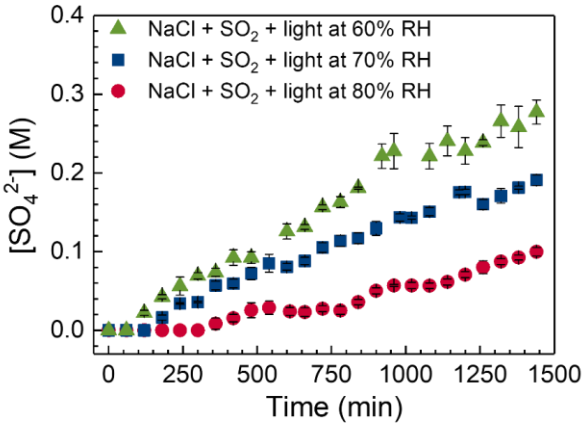

Figure S11. Sulfate concentration as a function of time during the uptake of SO_2 into NaCl droplets under irradiation at different RHs.

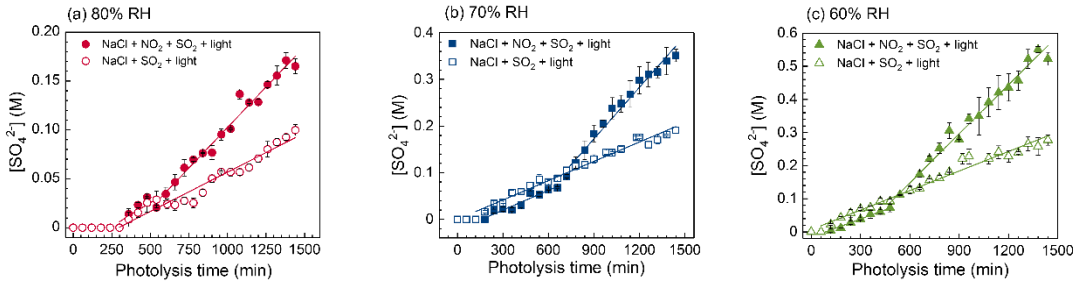

Figure S12. Sulfate concentration as a function of photolysis time at (a) 80% RH, (b) 70% RH, and (c) 60% RH.

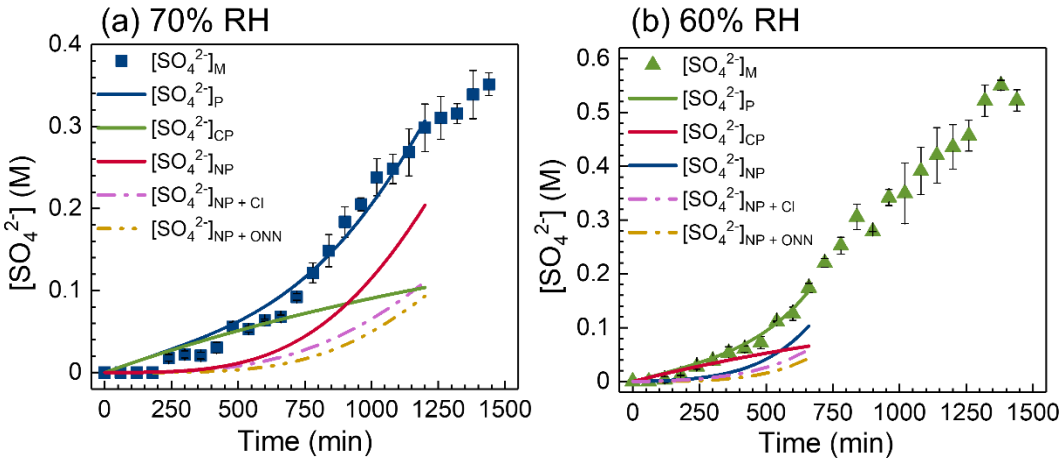

Figure S13. Model prediction of sulfate concentration under various conditions at 60% and 70%RH.

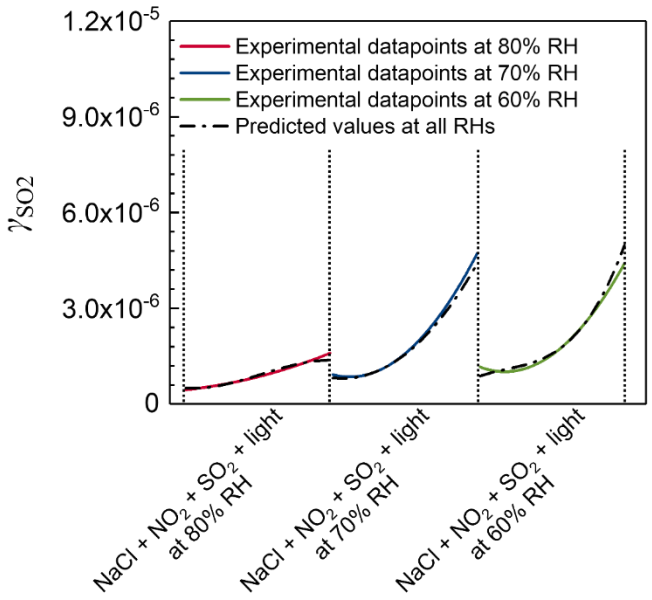

Figure S14. The γ_{SO2} from experiments NaCl + NO_2 + SO_2 + light at 80%, 70%, and 60% RH and predicted γ_{SO2} from the derived expression of γ_{SO2} = 0.41 × P_{NO3^-} + 0.34 × P_{Cl^-}.

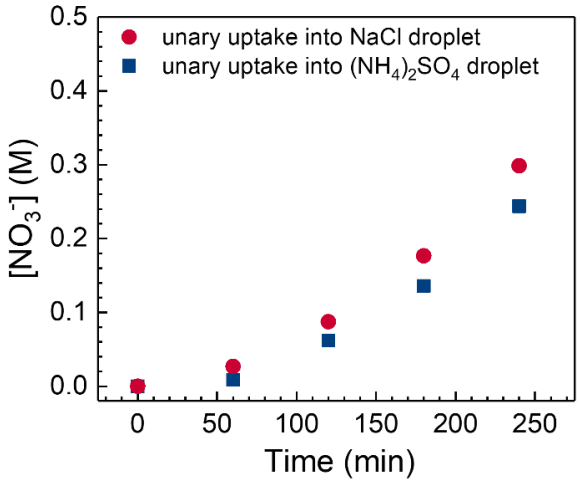

Figure S15. Unary uptake of NO_2 into NaCl droplets and $(NH_4)_2SO_4$ droplets at 80% RH under dark.

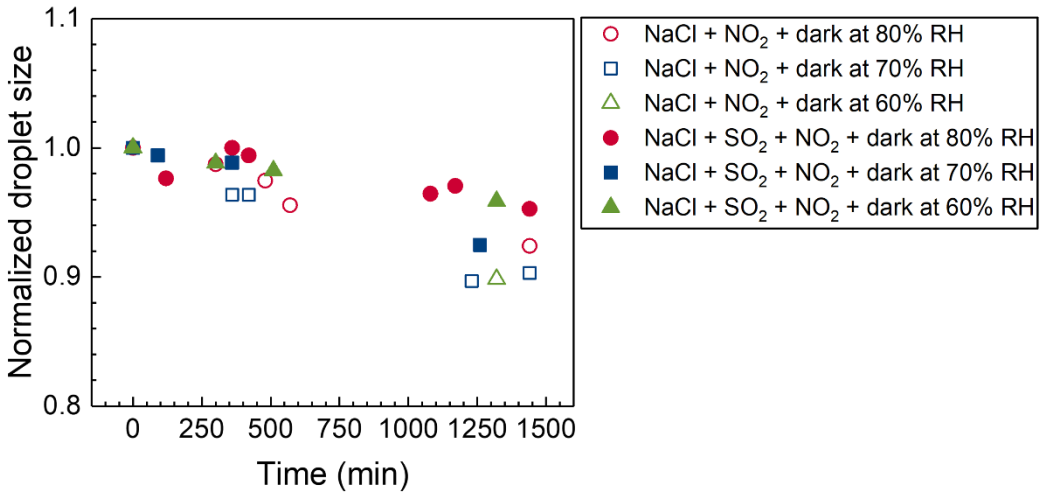

Figure S16. Normalized droplet size as a function of time under various conditions.

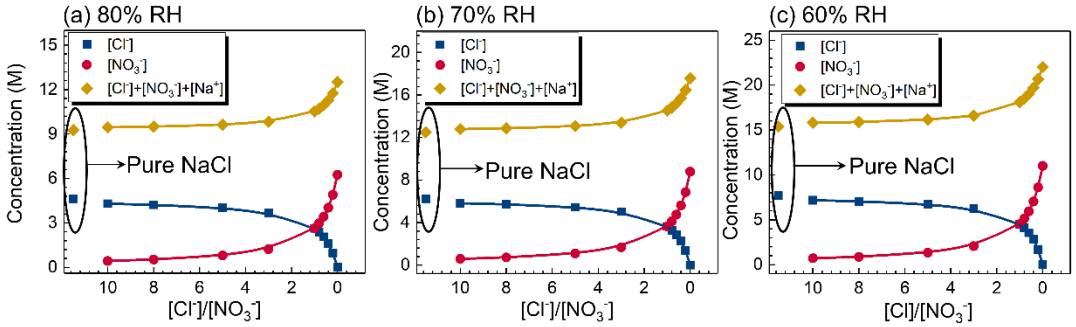

Figure S17. E-AIM model predicted nitrate, chloride, and total ions (represent ionic strength) concentration at different $[Cl^-]/[NO_3^-]$ at (a) 80% RH, (b) 70% RH, and (c) 60% RH.

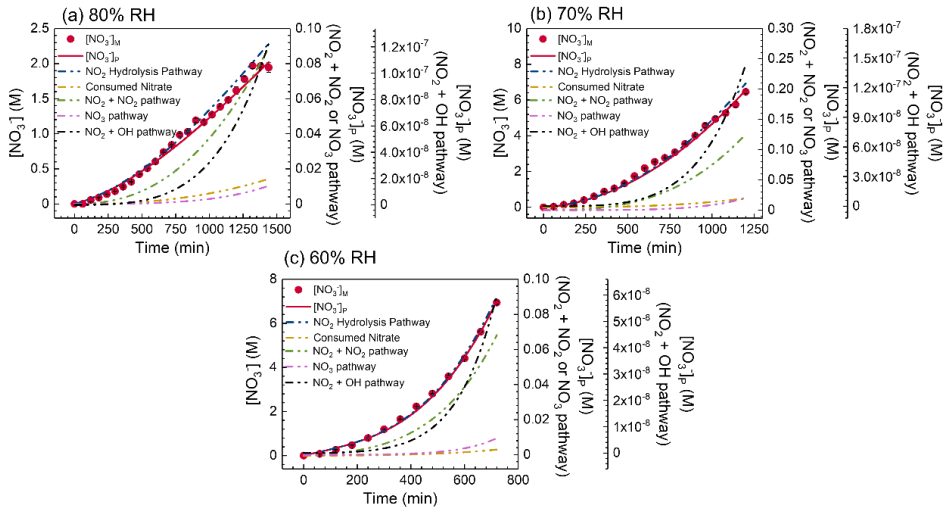

Figure S18. Model simulation of nitrate formation from unary uptake of NO_2 under irradiation.

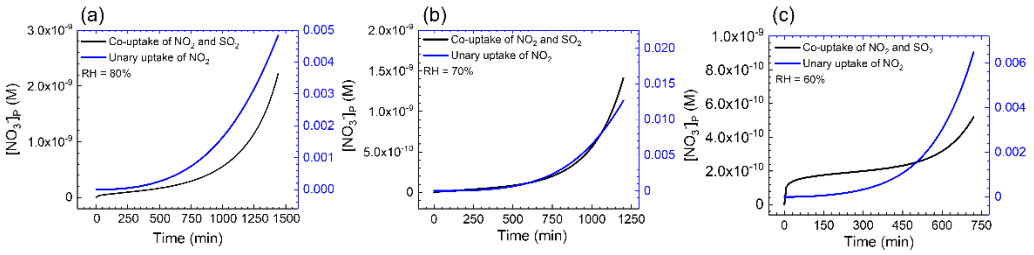

Figure S19. Nitrate from the reaction of Cl_2^- + NO_3 during unary uptake and co-uptake at (a) 80% RH, (b) 70% RH, and (c) 60% RH.

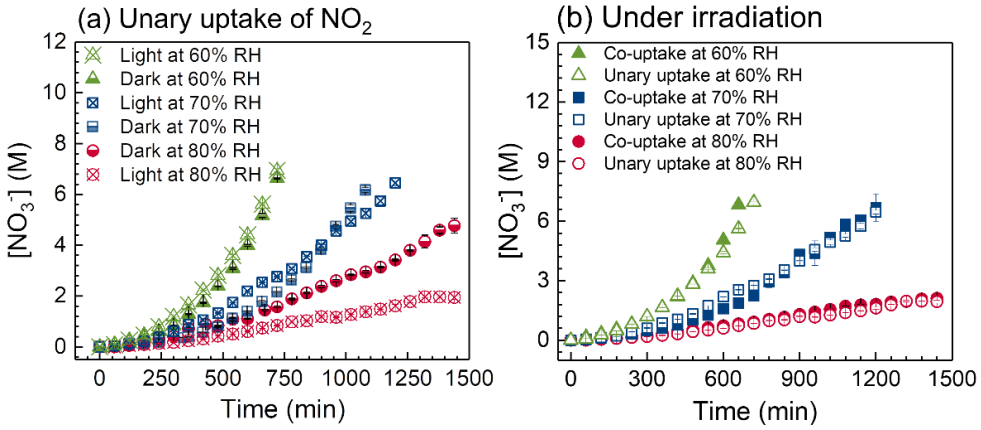

Figure S20. (a) Nitrate concentration as a function of time during unary uptake of NO_2 into NaCl droplets at all RHs. (b) The nitrate concentration as a formation of time at different RHs during co-/unary uptake under irradiation.

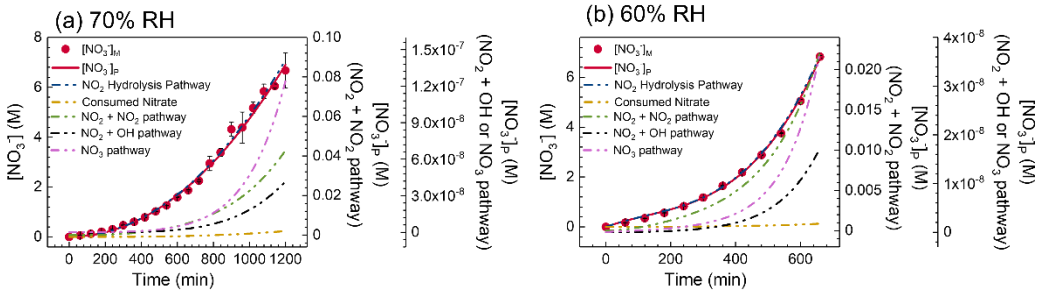

Figure S21. Model simulation of nitrate during co-uptake of NO_2 and SO_2 at 70% and 60% RH.

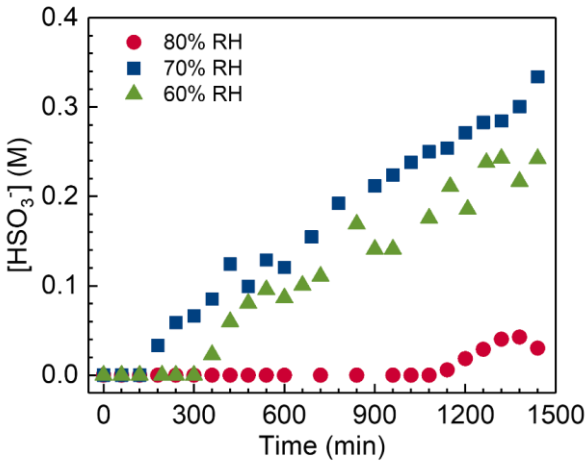

Figure S22. HSO_3^- concentration as a function of time at 60%, 70%, and 80% RH during unary uptake of SO_2 under dark. No sulfate was observed in these three conditions.

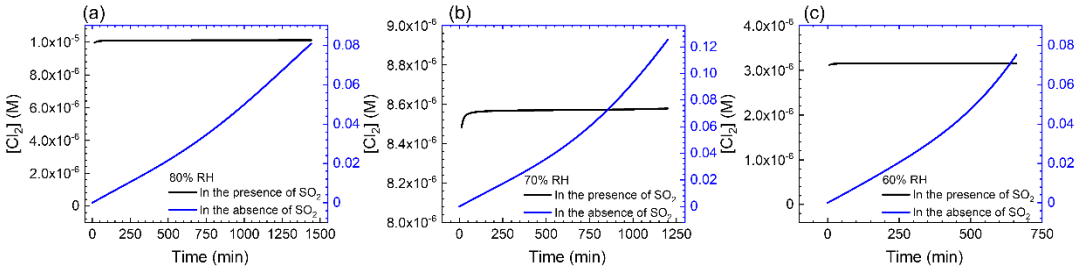

Figure S23. Estimated Cl_2 concentration in the presence and absence of SO_2 at all RHs.

Reference:

(1) Behnke, W.; George, C.; Scheer, V.; Zetzsch, C.: Production and decay of ClNO2 from the reaction of gaseous N2O5 with NaCl solution: Bulk and aerosol experiments. J. Geophys. Res. Atmos., 102, 3795-3804, 1997.
(2) Benner, C. L.; Eatough, N. L.; Lewis, E. A.; Eatough, D. J.; Huang, A. A.; Ellis, E. C.: Diffusion coefficients for ambient nitric and nitrous acids from Denuder experiments in the 1985 nitrogen species methods comparison study. Atmos. Environ., 22, 1669-1672, doi.org/https://doi.org/10.1016/0004-6981(88)90395-2, 1988.
(3) Bulman, D. M.; Mezyk, S. P.; Remucal, C. K.: The impact of pH and irradiation wavelength on the production of reactive oxidants during chlorine photolysis. Environ. Sci. Technol., 53, 4450-4459, 2019.
(4) Buxton, G. V.; Greenstock, C. L.; Helman, W. P.; Ross, A. B.: Critical Review of rate constants for reactions of hydrated electrons, hydrogen atoms and hydroxyl radicals (· OH/· O− in Aqueous Solution. J. Phys. Chem. Ref. Data, 17, 513-886, 1988.
(5) Galib, M.; Limmer, D. T.: Reactive uptake of N2O5 by atmospheric aerosol is dominated by interfacial processes. Science, 371, 921-925, 2021.
(6) Gen, M.; Zhang, R.; Huang, D. D.; Li, Y.; Chan, C. K.: Heterogeneous Oxidation of SO2 in Sulfate Production during Nitrate Photolysis at 300 nm: Effect of pH, Relative Humidity, Irradiation Intensity, and the Presence of Organic Compounds. Environ. Sci. Technol., 53, 8757-8766, doi.org/10.1021/acs.est.9b01623, 2019.
(7) Griffiths, P. T.; Badger, C. L.; Cox, R. A.; Folkers, M.; Henk, H. H.; Mentel, T. F.: Reactive uptake of N2O5 by aerosols containing dicarboxylic acids. Effect of particle phase, composition, and nitrate content. J. Phys. Chem. A, 113, 5082-5090, 2009.
(8) Gutzwiller, L.; George, C.; Rössler, E.; Ammann, M.: Reaction Kinetics of NO2 with Resorcinol and 2,7-Naphthalenediol in the Aqueous Phase at Different pH. J. Phys. Chem. A, 106, 12045-12050, doi.org/10.1021/jp026240d, 2002.
(9) Horváth, A. K.; Nagypál, I.; Epstein, I. R.: Three Autocatalysts and Self-Inhibition in a Single Reaction: A Detailed Mechanism of the Chlorite− Tetrathionate Reaction. Inorg. Chem., 45, 9877-9883, 2006.
(10) Huie, R. E.; Neta, P.: Rate constants for some oxidations of S (IV) by radicals in aqueous solutions. Atmos. Environ., 21, 1743-1747, 1987.
(11) Katsumura, Y.; Jiang, P.; Nagaishi, R.; Oishi, T.; Ishigure, K.; Yoshida, Y.: Pulse radiolysis study of aqueous nitric acid solutions: formation mechanism, yield, and reactivity of NO3 radical. J. Phys. Chem., 95, 4435-4439, 1991.
(12) Klaning, U. K.; Sehested, K.; Appelman, E. H.: Laser flash photolysis and pulse radiolysis of aqueous solutions of the fluoroxysulfate ion, SO4F. Inorg. Chem., 30, 3582-3584, 1991.
(13) Kläning, U. K.; Sehested, K.; Wolff, T.: Ozone formation in laser flash photolysis of oxoacids and oxoanions of chlorine and bromine. Journal of the Chemical Society, Faraday Transactions 1: Physical Chemistry in Condensed Phases, 80, 2969-2979, 1984.
(14) Kolb, C.; Davidovits, P.; Jayne, J.; Shi, Q.; Worsnop, D.: Kinetics of trace gas uptake by liquid surfaces. Prog. React. Kinet. Mech., 27, 1-46, 2002.
(15) Li, P.; Pang, H.; Wang, Y.; Deng, H.; Liu, J.; Loisel, G.; Jin, B.; Li, X.; Vione, D.; Gligorovski, S.: Inorganic Ions Enhance the Number of Product Compounds through Heterogeneous Processing of Gaseous NO2 on an Aqueous Layer of Acetosyringone. Environ. Sci. Technol., 56, 5398-5408, doi.org/10.1021/acs.est.1c08283, 2022.
(16) Løgager, T.; Sehested, K.; Holcman, J.: Rate constants of the equilibrium reactions SO⁻ 4+ HNO3⇄ HSO-4+ NO. 3 and SO⁻ 4+ NO-3⇄ SO2-4+ NO. 3. Radiat. Phys. Chem., 41, 539-543, 1993.
(17) Machulek, A.; Moraes, J. E. F.; Okano, L. T.; Silvérioc, C. A.; Quina, F. H.: Photolysis of ferric ions in the presence of sulfate or chloride ions: implications for the photo-Fenton process. Photochemical & Photobiological Sciences, 8, 985-991, 2009.
(18) Mekic, M.; Loisel, G.; Zhou, W.; Jiang, B.; Vione, D.; Gligorovski, S.: Ionic-strength effects on the reactive uptake of ozone on aqueous pyruvic acid: Implications for air–sea ozone deposition. Environ. Sci. Technol., 52, 12306-12315, 2018.
(19) Poskrebyshev, G.; Huie, R.; Neta, P.: The rate and equilibrium constants for the reaction NO3•+ Cl-⇄ NO3-+ Cl• in aqueous solutions. J. Phys. Chem. A, 107, 1964-1970, 2003.

(20) Scharko, N. K.; Berke, A. E.; Raff, J. D.: Release of nitrous acid and nitrogen dioxide from nitrate photolysis in acidic aqueous solutions. Environ. Sci. Technol., 48, 11991-12001, 2014.
(21) Sehested, K.; Holcman, J.; Bjergbakke, E.; Hart, E. J.: A pulse radiolytic study of the reaction hydroxyl+ ozone in aqueous medium. J. Phys. Chem., 88, 4144-4147, 1984.
(22) Seinfeld, J. H.; Pandis, S. N. J. I., New York: Atmospheric chemistry and physics: From air pollution to climate change, John Willey & Sons. 2006.
(23) Stewart, D. J.; Griffiths, P.; Cox, R.: Reactive uptake coefficients for heterogeneous reaction of N 2 O 5 with submicron aerosols of NaCl and natural sea salt. Atmos. Chem. Phys., 4, 1381-1388, 2004.
(24) Yu, X.-Y.; Barker, J. R.: Hydrogen peroxide photolysis in acidic aqueous solutions containing chloride ions. I. Chemical mechanism. J. Phys. Chem. A, 107, 1313-1324, 2003.
(25) Zhang, R.; Gen, M.; Fu, T.-M.; Chan, C. K.: Production of Formate via Oxidation of Glyoxal Promoted by Particulate Nitrate Photolysis. Environ. Sci. Technol., 55, 5711-5720, doi.org/10.1021/acs.est.0c08199, 2021.
(26) Zhang, R.; Gen, M.; Huang, D.; Li, Y.; Chan, C. K.: Enhanced Sulfate Production by Nitrate Photolysis in the Presence of Halide Ions in Atmospheric Particles. Environ. Sci. Technol., 54, 3831-3839, doi.org/10.1021/acs.est.9b06445, 2020.